COMPOSITES & POLYCON 2009
American Composites Manufacturers Association
January 15-17, 2009
Tampa, FL USA

Modeling of Composite Panel Under Fire and Compression

By

Ziqing Yu, Dept of Engineering Technology
Aixi Zhou, Dept of Engineering Technology
University of North Carolina at Charlotte

Abstract

A two dimensional coupled thermo-mechanical finite element (FE) model is developed to simulate the behavior of a composite panel under simultaneous furnace fire and compressive mechanical load. The objective is to develop FE models that can provide reasonable estimation of temperature profile and history, deformation history, failure modes, and time-to-failure of a composite panel subject to fire and compression. The composite panel is made from E-glass/Vinyl Ester through the VARTM process. Temperature-dependent thermal and mechanical properties are considered in FE modeling. Parametric studies on both thermal and mechanical boundaries are carried out to investigate the effects of thermal and mechanical boundary conditions on the behavior of the composite panel in fire. Possible failure modes including material degradation, structural stability, compressive strength, and excessive deformation are discussed and failure criteria are provided for time-to-failure estimations. Results from the FE modeling are in close agreement with available experimental data.

1 Introduction

Fiber Reinforced Polymer (FRP) composites have many advantageous properties, such as high specific strength, tailorable mechanical and physical properties, excellent part integration, enhanced resistance to fatigue and environmental attacks, and reduced life-cycle costs. However, because the resins are polymers, FRP composites are combustible. Therefore, fire safety is of great concern for these materials.

Recently, FRP composites have been increasingly used in structures where fire safety requirements are stringent, such as aircraft structures, naval ships, and building structures. In these applications, FRP composite structures are designed to carry structural loads. Therefore, it is desirable to predict the structural integrity and possible failure modes of these FRP structures in fire, and estimate time-to-failure of these composite structures.

This paper presents a study on modeling a marine grade E-glass/Vinyl Ester composite panel subject to simultaneous furnace fire and mechanical compressive load. In FE modeling, temperature-dependent thermal and mechanical properties are used to consider material degradation from fire damage and decomposition. To investigate the effects of thermal and mechanical boundary conditions on the behavior of composite panel in fire, series parametric studies on both thermal and mechanical boundaries are performed. Failure modes including material degradation, structural stability, material strength, and excessive deformation are discussed and failure criteria are provided for time-to-failure estimations. The modeling and analytical work is compared with medium scale structural fire testing on the same composite panels.

2 Temperature Dependent Material Property Models

Previous research (1-8) showed that empirical progressive softening model can be used to consider the loss in stiffness and strength of a decomposing FRP composite laminate. It is assumed that the mechanical properties vary in the through-thickness direction due to the temperature gradient through the laminate. The dependence of the compressive stiffness and strength on temperature must be known to calculate the time-to-failure using the progressive softening model.

The typical relationship between the mechanical property of a laminate and temperature is shown in Figure 1. The mechanical property remains at the room temperature value, P_u, until the laminate is heated to a critical softening temperature (T_{cr}), above which the property decreases with increasing temperature to a "minimum value" (P_R). This reduction is due to thermal softening of the polymer matrix as it undergoes glass transition. The mechanical properties including Young's modulus, shear modulus, and compressive strength all show similar temperature dependence as shown in Figure 1. (1)

For analysis and FE modeling of a composite structure, it is desirable to develop an analytical equation describing temperature dependence of mechanical properties. Mouritz et. al (2) used the following hyperbolic tangent function to

approximate the relationship between mechanical properties and temperature before pyrolysis:

$$P(T) = \{\frac{P_U+P_R}{2} - \frac{P_U-P_R}{2}\tanh\big(\varphi\big(T-T_g\big)\big)\}R_{rc}(T)^n \quad (1)$$

Where P is the particular mechanical property, while P_U and P_R are the unrelaxed (room temperature) and relaxed (high temperature) values of that property. The values of P_U and P_R for the laminate must be measured by experimental testing; T is the temperature; T'_g is the mechanically determined glass transition temperature, at which mechanical properties are half reduced compared with those at room temperature. In general, T'_g is not the same for all properties; φ is a constant describing the breadth of the distribution; $R_{rc}(T)^n$ is a power law factor to account for effects of pyrolysis on the mechanical properties of laminate .The exponent *n* is a constant dependent on the relationship between mass loss of the resin matrix and the mechanical property. When $n = 0$ it is assumed that resin decomposition has no affect on the mechanical property. When $n = 1$ it is assumed that a linear relationship exists between mass loss and the property. Other values of *n* can be used to describe nonlinear relationships between mass loss and residual.

3 Finite Element Analysis Implementation

In this section we present a finite element analysis of deflection and temperature histories of the composite panel. This problem has been studied in a series of structural fire tests (9), and will serve as a comparison to numerical results. Geometry and loading in the tests are shown in Figure 2. For simplicity, plane strain and one dimensional heat transfer through the thickness direction are assumed to model the problem. A two dimensional (2D) finite element model (Figure 3) in ABAQUS is developed to predict the temperature profile/history and in-plane and out-of-plane deflections. The model is a coupled thermal-mechanical analysis, where the temperature profile distribution is calculated and then the panel deformation is determined based on the temperature field and the mechanical properties, which are temperature dependent.

3.1 Material properties

The laminate used in structural fire testing and FE modeling was fabricated using 24 oz./yd² plain weave E-glass fiber fabrics and vinyl ester resin. When the mechanical properties are fit using Eq (1), φ is 0.038 and T´g is 123ºC for compressive modulus, the compressive modulus at room temperature is 20.67 GPa; For shear modulus fitting, φ is 0.035 and T´g is 77ºC, the room-temperature shear modulus is 3.8 GPa. The decomposition factor F(T) is used to account for effects of decomposition, where F(T) is defined by

$$\mathrm{F(T)} = (\rho_\mathrm{T} - \rho_\mathrm{f})/\rho_0 \quad (2)$$

where ρ_T, ρ_f, ρ_0 are the temperature dependent, final, and original densities; ρ_T is assumed to be a function of temperature only. Therefore, the material model in this study is given by

$$E_x = \left\{\frac{20.67+13}{2} - \frac{20.67-13}{2}\tanh\big(0.038(T-123)\big)\right\}F(T)^3 \quad (3)$$

where T is instantaneous temperature; n in Eqn (1) is 3 for E-glass Vinyl Ester as validated by Mouritz et. al (2)

Since super wool is used for heat insulation only, its Young's Modulus and Poisson's rate in ABAQUS are taken as 1Pa and 0.3 respectively.

Temperature-dependent thermal properties will be used for the E-glass/Vinyl Ester panel (Figure 4 and 5); Specific heat capacity and thermal conductivity of super wool are given by

$$\mathrm{C_p} = -1.17\times10^{-4}\mathrm{T}^2 + 0.416\mathrm{T} + 776.4 \quad (3)$$
$$\mathrm{k} = 1.48\times10^{-7}\mathrm{T}^2 + 1.79\times10^{-4}\mathrm{T} + 1.28\times10^{-2} \quad (4)$$

Where, T is temperature, C_p is specific heat capacity (J/kg.K), k is thermal conductivity (W/m.K)

3.2 FE models in ABAQUS

A 2D coupled thermal-mechanical finite element model in ABAQUS is developed to predict the temperature profile/history and out-of-plane deflection.

3.2.1 Mechanical Boundary Conditions

The experimental setup in Figure 2 was intended for a clamped boundary condition on the top end and a simply supported boundary condition for the bottom end of the composite panel. However, due to thermal expansion of the ends during fire testing, the actual end fixing conditions varied from the intent. To investigate the effects of different boundary conditions on the behavior of the composite panel, simply supported and clamped boundary conditions are applied to top and/or bottom surfaces in different FEA models. The results from these FEA models will be compared with experimental data. The model represents the closest behavior of the panel will be considered as the actual boundary condition of the panel during fire testing.

For top surface, simply supported boundary only constrains the surface's translational freedom in thickness direction (U_z):

$$U_z = 0 \quad (5)$$

While clamped boundary constrains both the surface's rotation freedom (UR_y) and translational freedom in the thickness direction (U_z):

$$U_z = 0 \text{ and } UR_y = 0 \quad (6)$$

For bottom surface, simply supported boundary allows all freedoms except for translation of the surface's middle point:

$$U_x = U_y = U_z = 0 \quad (7)$$

While clamped boundary fixes all freedoms of the surface:

$$U_x = U_y = U_z = UR_x = UR_y = UR_z = 0 \quad (8)$$

3.2.2 Thermal Boundary Conditions

In experiments, furnace temperature varied according the standard time-temperature curve, IMO A.754 (18) fire curve (9). Since from experiments the temperature of the left surface (hot surface of super wool insulation layer) is very close to that of furnace (Figure 13), temperature boundary instead of real heat transfer boundary will be applied directly to the left surface based on the standard time-temperature curve (IMO A.754). Convection and radiation boundary is used for the right surface (cold surface of laminate). Other surfaces are taken as thermally insulated (i.e. no radiation and convection effects) because the panel is very thin.

As suggested by ASTM (10), the convective heat transfer coefficient for exchange between a turbulent air flow and a vertical surface can be approximated as follows:

$$h = 0.95(\Delta T)^{1/3} \quad (9)$$

where, h = W/m².K and ΔT = temperature difference between the vertical surface and the air. Also in ASTM (10), Some fire models use a fixed convective coefficient of approximately 10 W/m².K or a linear function of temperature to calculate convective coefficient. For effects of heat radiation, it's common to use 0.95 for radiation emissivity of composite materials

3.2.3 Loading History

FEA comparison studies showed no significant differences between results obtained from a concentrated force and results obtained from a distributed nodal stress with the same resultant compression force. For simplicity, a concentrated force of 9.9 kN was applied for all models on the middle point of top surface for 70 minutes or longer.

Based on knowledge above, four models (Table 1) with different mechanical and same thermal boundary on the right surface are defined to evaluate mechanical boundaries' effects on temperature field and deflection history. To obtain thermal boundaries' effects on temperature and deflection solutions, different thermal boundaries and same simply-supported boundary will be used in four models (Table 2).

The finite element model consists of 8645 4-node linear coupled temperature-displacement plane strain elements (CPE4RT) with reduced integration and hourglass control (11). In the following simulation, six elements are used in the through-thickness direction. A nonlinear coupled temperature-displacement analysis step in ABAQUS is used with 5ºC maximum allowable temperature change per time increment.

Model 1 (Table 1) is rerun with 24 elements through the thickness direction and 1ºC maximum allowable temperature change per time increment for convergence studies. Almost same results are obtained, indicating temperature and deflection solutions are convergent.

4 Results and Discussions

4.1 Results

All results from FE modeling are plotted together with experimental data. Figures 6 to 8 show the effect of different supporting boundaries on deflections of three specific points. Simply supported boundaries (Model 1 in Table 1) give the closest deflection results to experimental data.

Figures 9-13 show the predicted temperature profiles in comparison with experimental data for three locations throughout the laminate thickness. It can be seen that on average Model 8 gives the best predictions for the various locations. Convection only models (Model 5 and Model 6) generally produce higher temperatures within the laminate as the heat loss through the cold face is reduced. Convection and radiation leads to a higher heat loss and compares best to the experimental temperature profiles.

Figures 14 to 17 show the effect of different thermal boundaries on both in-plane and out-of-plane deflections. The models initially result in similar deflection patterns. The agreement prior to 30 minutes is good. Convection-only Models 5 and 6 (Table 2) predict earlier buckling failure than Models 7 and 8, which include effects of heat radiation. The good consistency between temperature and deflection results is indicated by the fact that Model 8 gives the best temperature and deflection predictions. Models 5 and 6 overestimated the temperature and predicted shorter times of buckling failure, and Model 7 underestimated the temperature gave a longer time of failure.

Based on the analysis, it can be concluded that the failure predictions for buckling are very sensitive to the degradation of the Young's modulus at higher temperatures (temperature range 200- 400°C based on temperature differences between the models).

4.2 Failure Criteria and Time-to-Failure Predictions

The time-to-failure predictions depend on the failure modes and failure mechanisms of the composite panel. In the following, several failure criteria are used to provide time-to-failure predictions.

4.2.1 Time-to-Failure Prediction Using Stability Criterion

Buckling failure is a common failure mode for beam or shell structures under compression, which is indicated by a large response caused by a small additional axial or lateral disturbance applied to the structure. In Abaqus, both transient and static steps can be used to implement nonlinear stability analysis. For a model with perfectly symmetric geometry, boundary conditions, and loading history, imperfection and/or perturbations must be introduced to "initiate" buckling. In this study, since the panel is under one-sided fire load, no additional perturbation is necessary. The deformation or deformation ratio history can be used to determine time of buckling. Here, deflection is used to identify buckling failure.

Figures 14-17 show buckling failure for Models 5-8. Time to failure given by Model 5 is 51 minutes; by Model 6 is 45 minutes; by Model 7 is 71 minutes; and by Model 8 is 58 minutes, which is the best model for buckling prediction.

4.2.2 Time-to-Failure Prediction Using Compressive Strength Criterion

Compressive failure is assumed to occur once the average compressive strength ($\boldsymbol{\sigma_{av}}$) is reduced to the compressive stress applied to the laminate. The time taken for the strength to decrease to the applied stress is taken to be the time-to-failure. At this point it's assumed that all the plies in the through-thickness direction fail at the same time. The average compressive strength is determined by integrating the strength values over the entire thickness of the laminate using the Simpson integration technique:

$$\sigma_{av} = \frac{1}{b-a}\int_a^b \sigma(x)dx = \frac{1}{3m}\left[\sigma(x_{0)} + 4\sigma(x_1) + 2\sigma(x_2) + \cdots + 2\sigma(x_{k-2}) + 4\sigma(x_{k-1}) + \sigma(x_k)\right] \quad (10)$$

Where m is the number of locations in the thickness direction where the residual compressive strength is calculated; m must be an even number. In this study, four points (TC2, TC3, TC4, and TC5) are used to calculate the average compressive strength.

Gibson et al. (4) expressed the temperature dependence of compressive strength using the semi-empirical equation:

$$\sigma_c(T) = \left(\frac{\sigma_c(o)+\sigma_c(R)}{2} - \frac{\sigma_c(o)-\sigma_c(R)}{2}\tanh\left(\varphi(T-T_k)\right)\right) R_{rc}(T)^n \quad (11)$$

Where φ is a material constant describing the temperature range over which the compressive strength is reduced during the thermal softening process; $\sigma_c(o)$ is compressive strength at room temperature; $\sigma_c(R)$ is "minimum value" at high temperature around 200ºC; F(T), the decomposition factor, can be also used to account for effects of mass loss on compressive strength. For a woven E-glass/vinyl ester laminate, $\sigma_c(o)$ is 435 MPa, $\sigma_c(R)$ is 9MPa.

Using temperature data from Model 8 in Table 2, Figure 19 shows compressive strength history. Compared with applied compressive stress (equivalent pressure of 1.16MPa for 70 minutes), no failure is predicted by compressive strength criterion.

4.2.3 Load Bearing Capacity

In ISO 834-1:1999(E), failure to support the load is deemed to have occurred for axially loaded structure when both of the following criteria have been exceeded.

Limiting axial contraction, $C = \frac{h}{100}$ mm; and

Limiting rate of axial contraction, $\frac{dC}{dt} = \frac{3h}{1000}$ mm/min;

where h is the initial height, in millimeters.

Figures 18-19 show that FE Model 8 predicts a failure time of 64.8 minutes, while the experimental data showed a failure time of 62.7 minutes. The comparison suggests a very good agreement between FE Model 8 and experiment.

4.2.4 Discussions

For composite structures under one-sided exposure to heat source, the temperature limit at cold side of the structure may be used to determine time-to-failure. When the temperature at cold side is higher than the glass transition temperature of the composite material, the structure is considered to be unsafe.

Since the temperature-limit criterion does not take into account effects of loading levels and temperature gradient, it does not work well in most cases.

Delamination has been observed as a failure mode of composite structures in fire. The cohesive element in Abaqus may be used to model delamination behavior of composite materials. Modeling of delamination of the composite panel in fire requires accurate temperature-dependent fracture

properties, appropriate introduced imperfections, and careful contact definition. Modeling delamination of composite in fire requires further investigation.

5 Conclusions

A 2D coupled thermomechanical FE model has been developed to consider temperature-dependent mechanical and thermal degradation of an E-glass/Vinyl Ester composite panel under combined fire and compressive loads. The FE modeling results compared well with available experimental data in terms of temperature profile and history as well as deformation history. Based on the validated FE modeling results, time-to-failure predictions are performed to consider several failure modes, including loss of structural stability, compressive strength degradation, and load carrying capacity. The modeling results show that end support conditions, thermal boundary conditions, and temperature-dependent Young's modulus play important roles in the structural response (stability) of panels in fire. Without considering decomposition of the composite resin explicitly, the FE modeling in general over-predicted temperatures in the laminate compared to experimental data. In future studies, accurate temperature-dependent compressive stiffness and strength, decomposition and delamination effect should be included in modeling work.

6 Acknowledgements

The authors wish to acknowledge the support of the US Office of Naval Research through the NICOP program under the direction of Dr. Luise Couchman, award # N00014-07-1-0514. The authors appreciate Dr. Kingshuk Bose of the Department of Mechanical Engineering at UNC Charlotte for valuable discussions.

Authors
Ziqing Yu, Research Assistant, Department of Engineering Technology, University of North Carolina at Charlotte.

Aixi Zhou, Assistant Professor, Department of Engineering Technology, University of North Carolina at Charlotte.

References

1. S. Feih et.al., Modelling the tension and compression strengths of polymer laminates in fire, Composites Science and Technology 67, 551–564 (2007).
2. A.P. Mouritz et.al., Mechanical property degradation of naval composite materials in fire, in Modeling of Naval Composite Structures in Fire, Edited by L. Couchman and A.P. Mouritz, Office of Naval Research, 51-106 (2006).
3. A.P. Mouritz and A.G. Gibson, Fire properties of polymer composite materials, Springer, 2006.
4. J. Kim et.al., Time-to-failure of compressively loaded composite structures exposed to fire, Journal of Composite Materials, 41, 2715 (2007).
5. J.V. Bausano et.al., Composite life under sustained compression and one sided simulated fire exposure: Characterization and prediction, Composites: Part A 37,1092 (2006).
6. P. Gu and R.J. Asaro, Structural buckling of polymer matrix composites due to reduced stiffness from fire damage, Composite Structures 69, 65 (2005).
7. A. Zhou and T. Keller, Structural responses of FRP elements under combined thermal and mechanical loadings: experiments and analyses. 4th Int. Conf. on the Response of Composite Materials to Fire, Newcastle, U.K., Sept. 15-16, 2005.
8. T. Keller, C. Tracy and A. Zhou, Structural response of liquid-cooled GFRP slabs subjected to fire: Part II. Thermo-chemical and thermo-mechanical modeling, Composites Part A, 37, (9), 1296 (2006).
9. B.Y. Lattimer et.al., Structural response of fiber reinforced plastic composites during fires, The 11th Interflam Conference, London, UK, 3-5 Sept., 2007 pp.653.
10. Standard Guide for Obtaining Data for Deterministic Fire Models, ASTM, Designation: E1591-07
11. Abaqus Analysis User's Manual, v6.7, Simulia Inc., Providence, RI, 2007
12. Terry L. Patterson, Illustrated 2003 Building Code Handbook, Chapter 16, Structural Design

Tables and Figures

Table 1 Models for Different Supporting Boundary Conditions

Models		1	2	3	4
Supporting BCs	Top	Simply Supported	Clamped	Simply Supported	Clamped
	Bottom	Simply Supported	Simply Supported	Clamped	Clamped
Thermal BCs	Left	Temperature Boundary: *IMO A.754*			
	Right	Convective h=0.95(T-20)^0.333, Radiation Emissivity 0.95			
Loading	Top	Concentrated force *9.9kN (equivalent 1.16 MPa)* for 70 minutes			

Table 2 Models for Different Thermal Boundary Conditions

Models		5	6	7	8
Supporting BCs		Top: Simply Supported; Bottom: Simply Supported			
Thermal BCs	Left Surface	Temperature Boundary: *IMO A.754*			
	Right Surface	**h=10*	$h = 0.95(T-30)^{\frac{1}{3}}$	*h=10* **e=0.95*	$h = 0.95(T-30)^{\frac{1}{3}}$ *e=0.95*
Loading	Top Surface	Concentrated force *9.9kN (equivalent 1.16 MPa)* for 70 minutes			

*h: convective coefficient; e: radiation emissivity

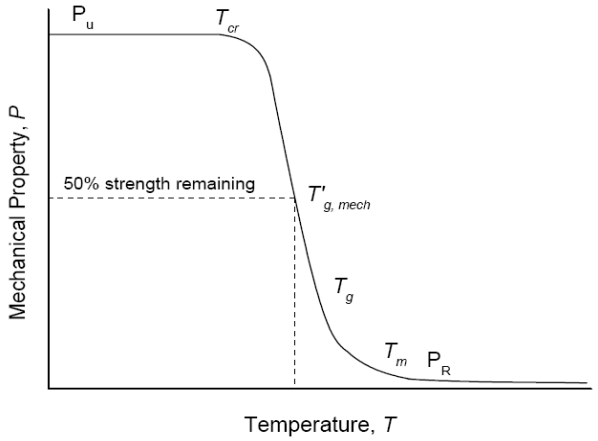

Figure 1 Effect of temperature on the compressive strength of a laminate

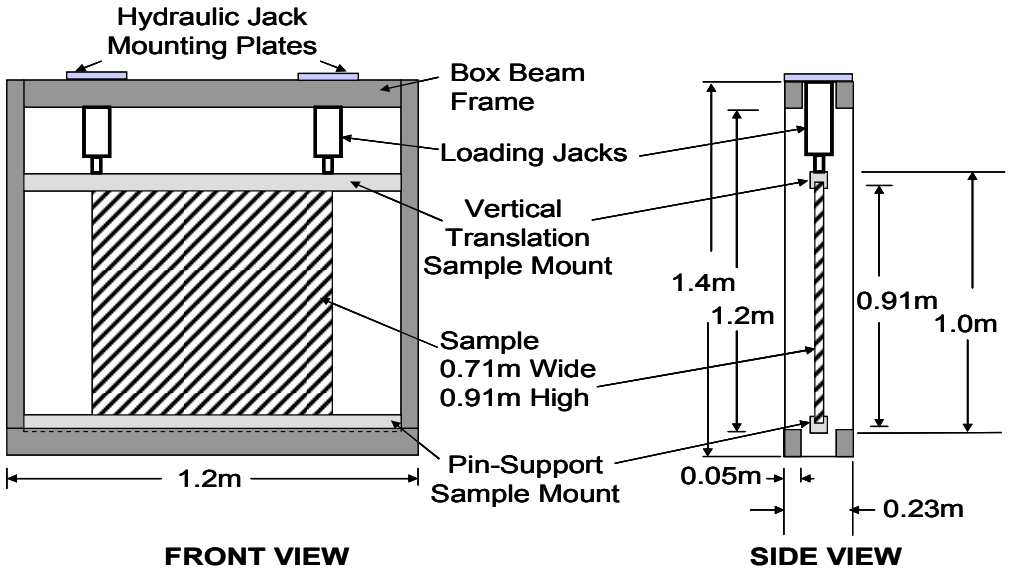

Figure 2 Geometry and loading in the test

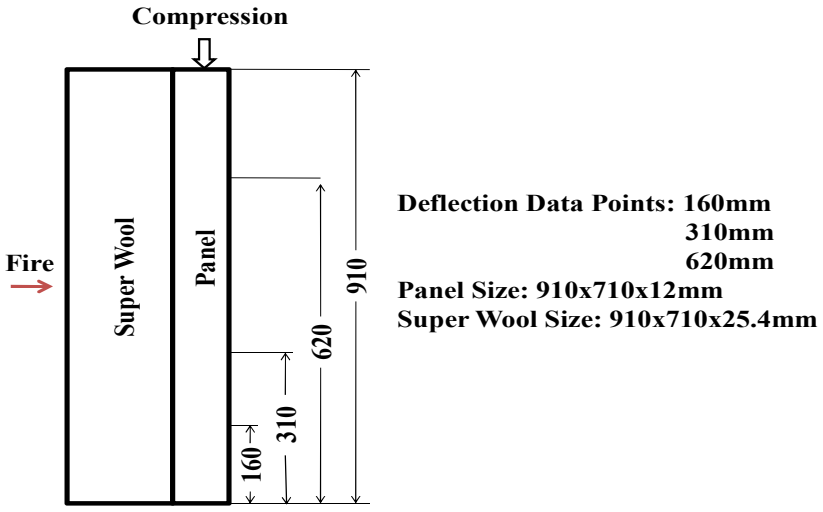

Figure 3 Geometry for FE Models

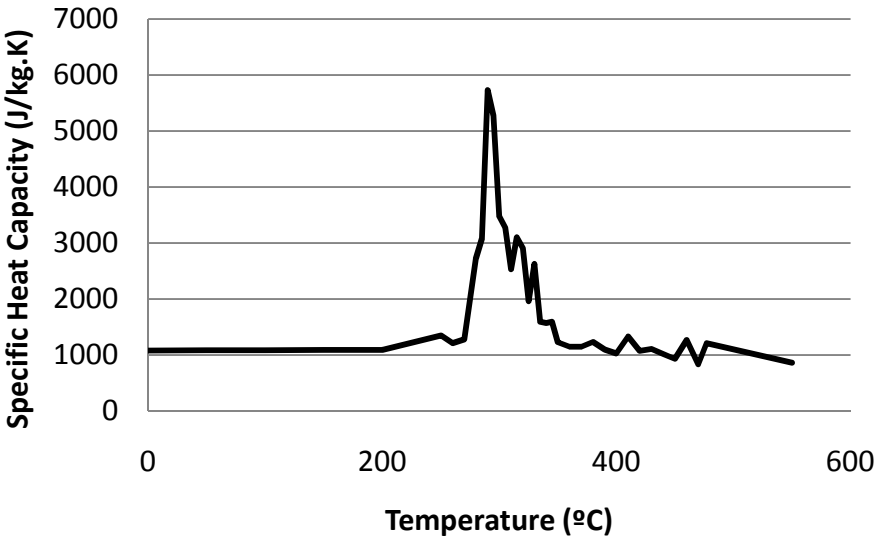

Figure 4 Specific Heat Capacity of E-glass/Vinyl Ester

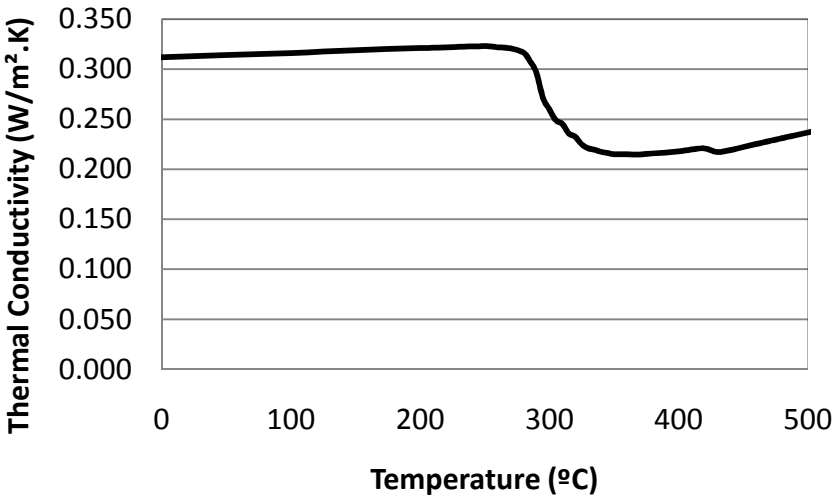

Figure 5 Thermal Conductivity of E-glass/Vinyl Ester

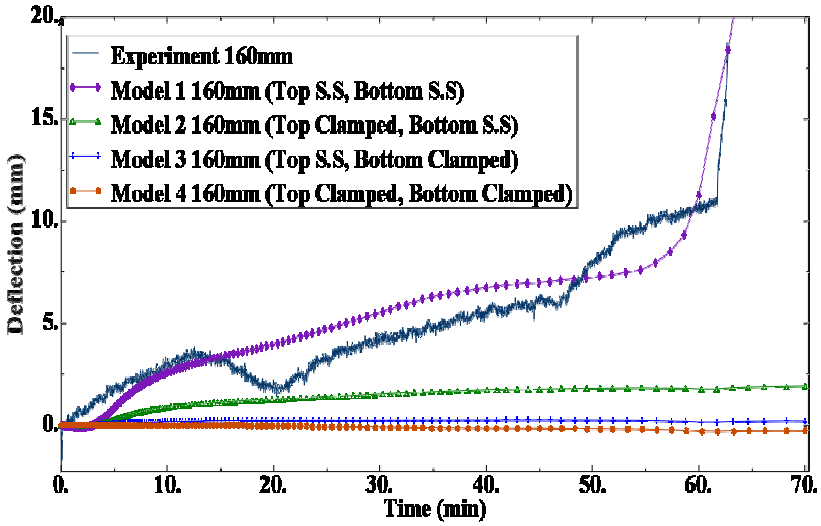

Figure 6 Deflection Comparisons at 160mm

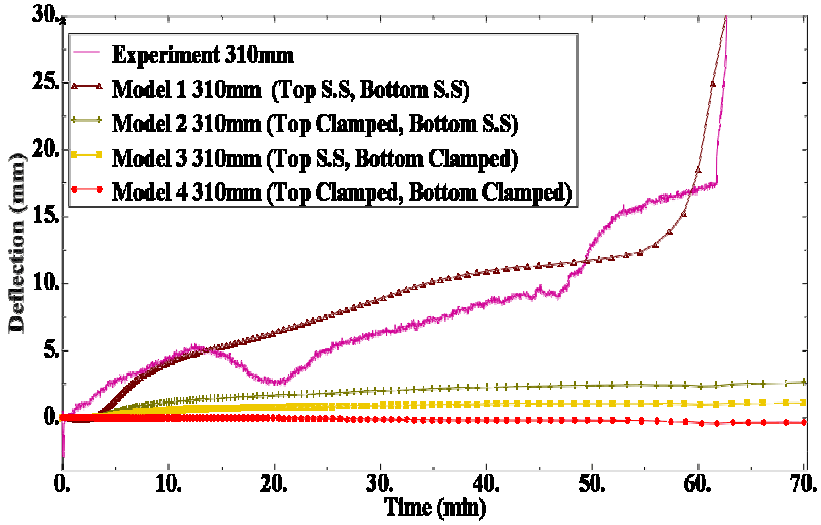

Figure 7 Deflection Comparisons at 310mm

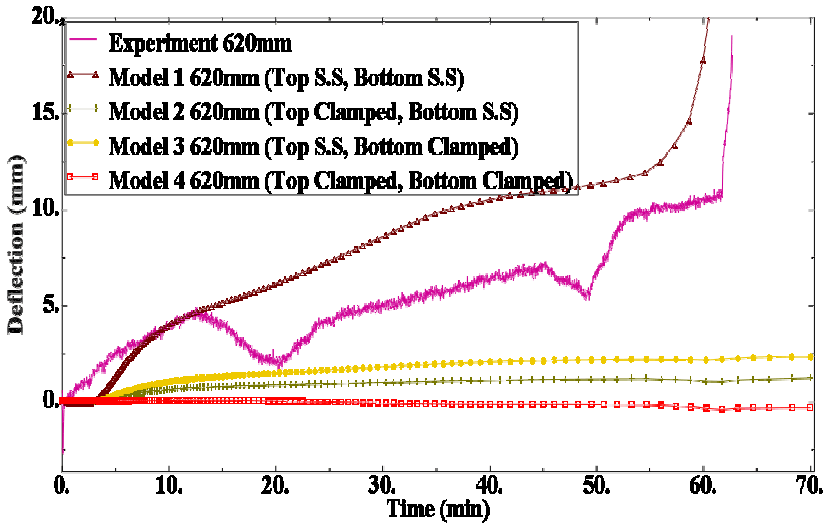

Figure 8 Deflection Comparisons at 620mm

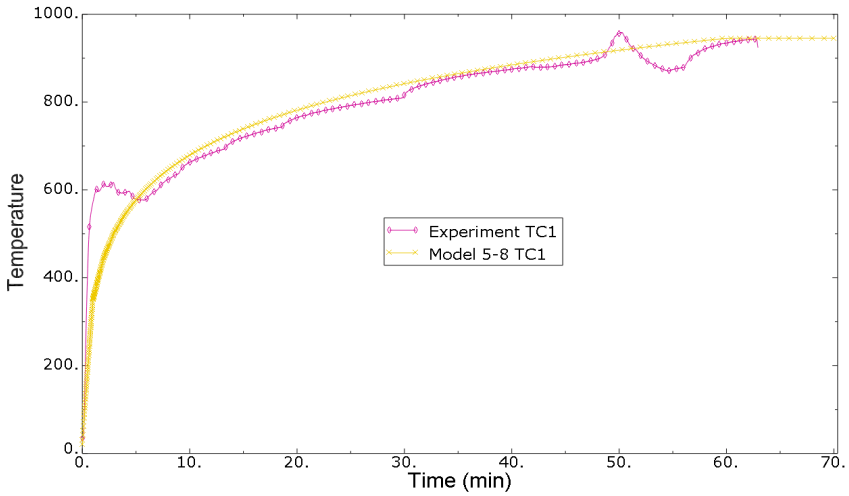

Figure 9 Temperature Comparisons at TC1

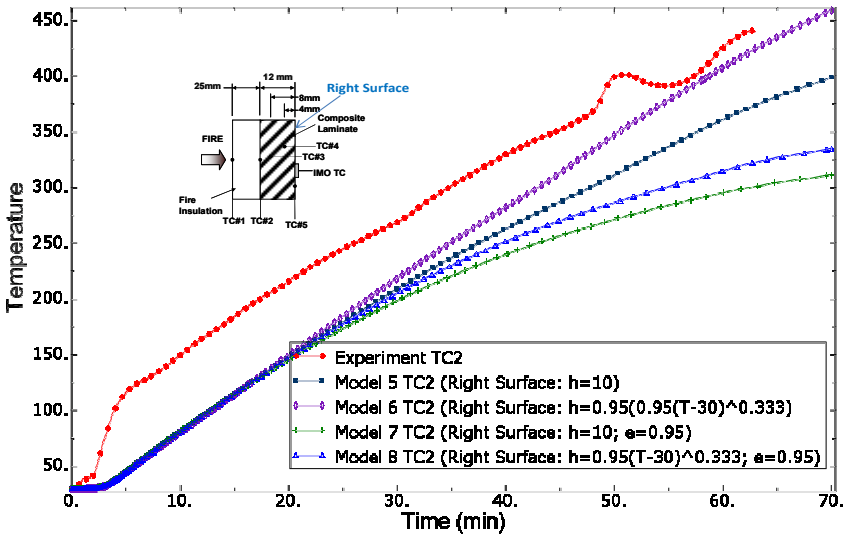

Figure 10 Temperature Comparisons at TC2

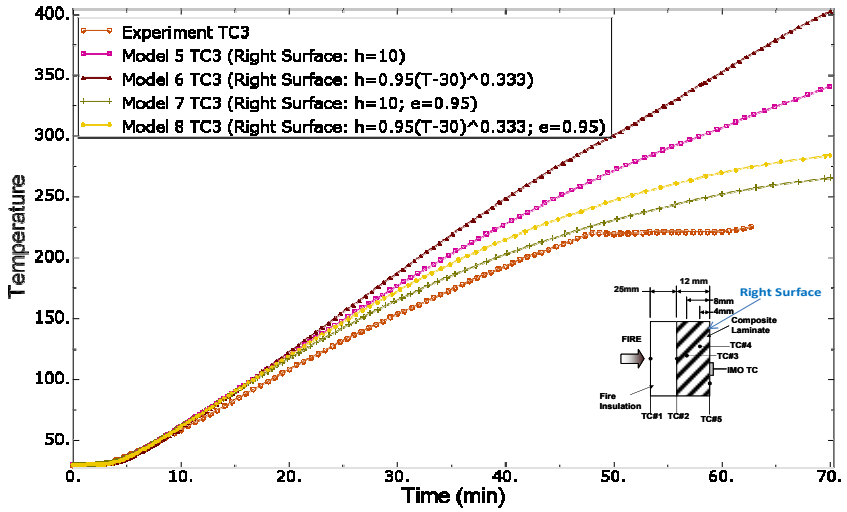

Figure 11 Temperature Comparison at TC3

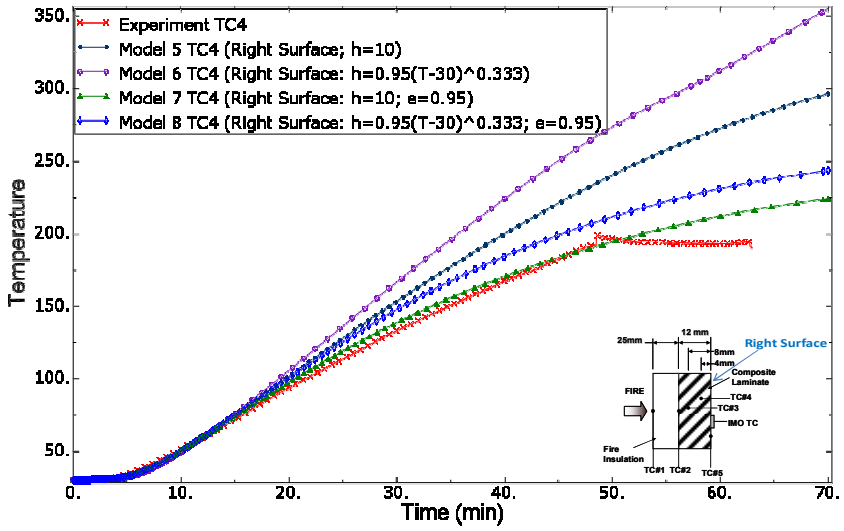

Figure 12 Temperature Comparison at TC4

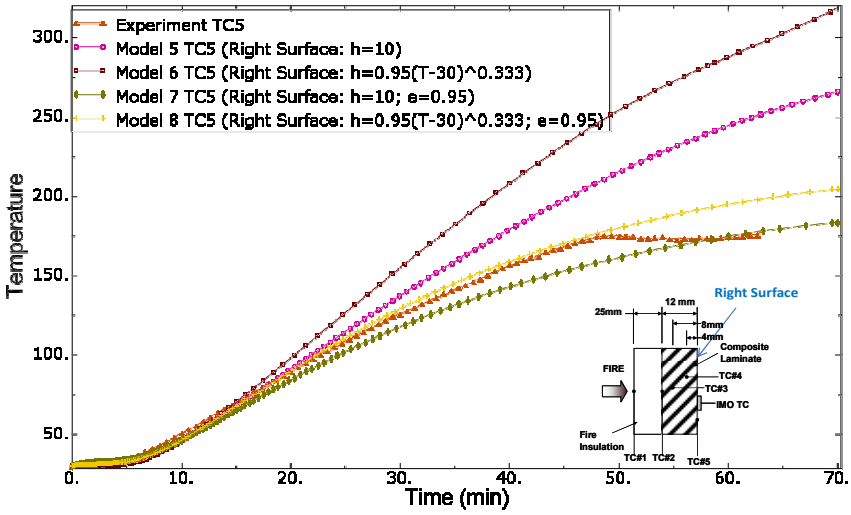

Figure 13 Temperature Comparison at TC5

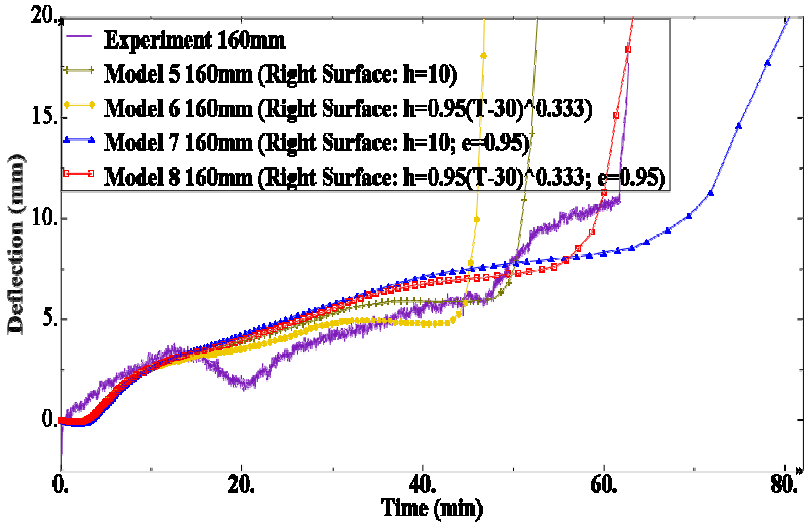

Figure 14 Deflection Comparisons at 160mm

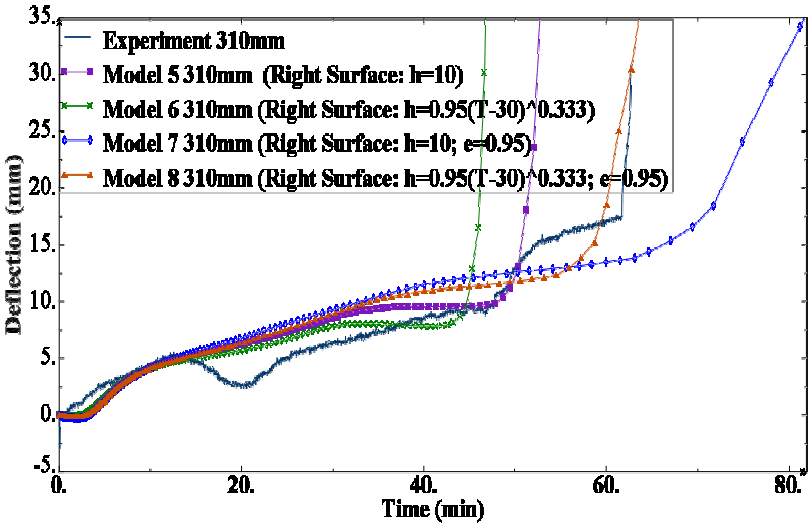

Figure 15 Deflection Comparisons at 310mm

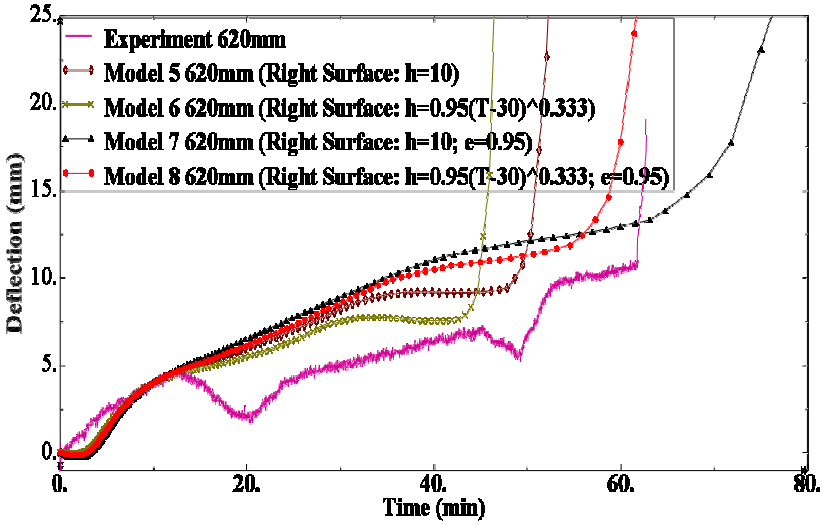

Figure 16 Deflection Comparisons at 620mm

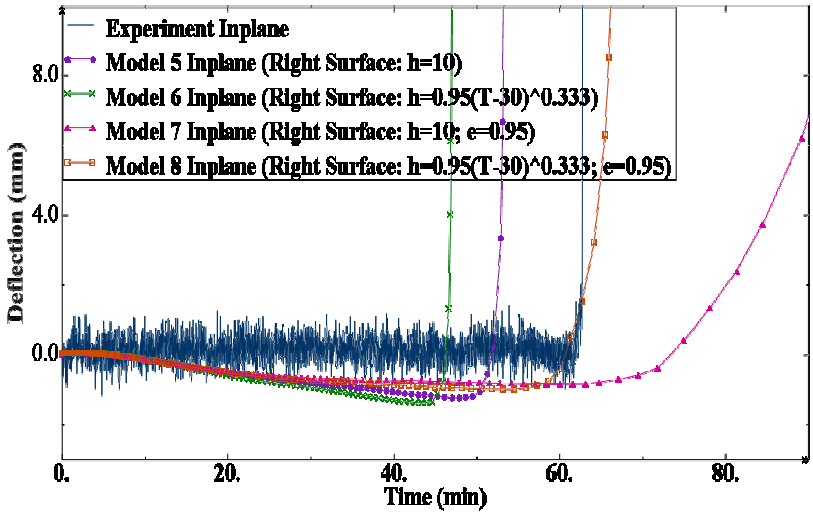

Figure 17 In-plane Displacement Comparison

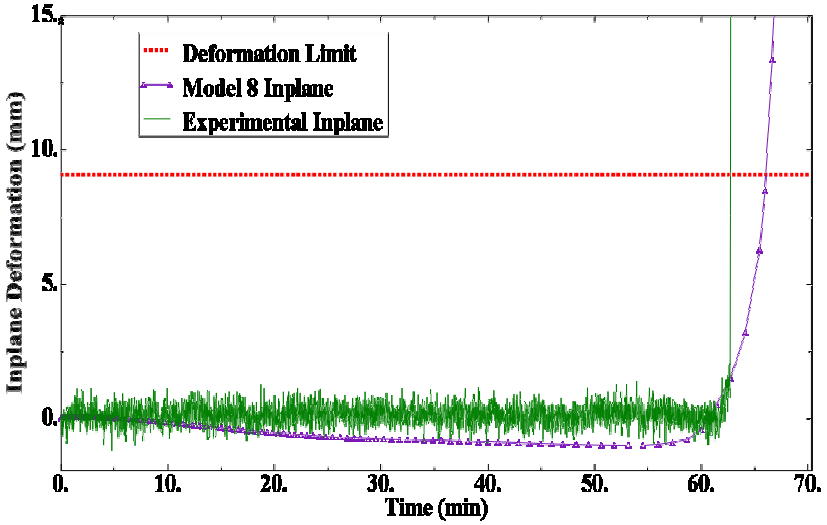

Figure 18 Aixal Contraction Comparisons

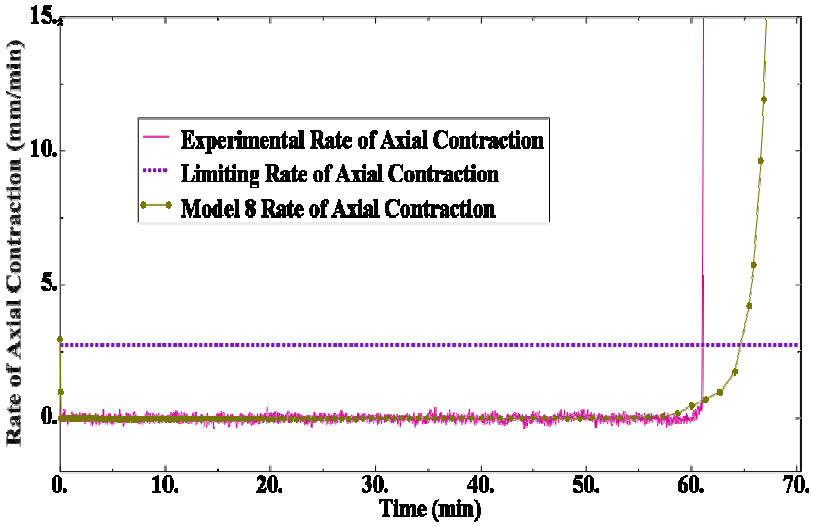

Figure 19 Rate of Axial Contraction Comparisons

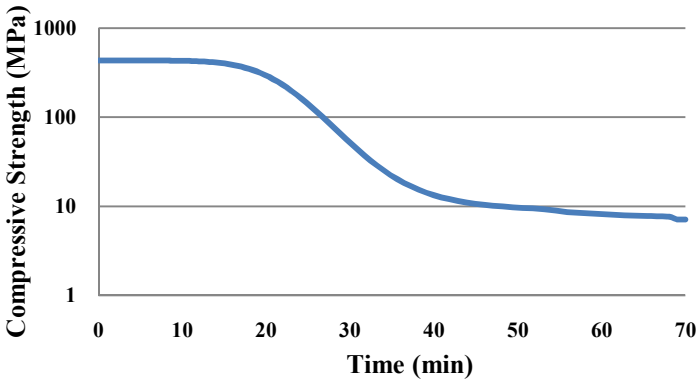

Figure 20 Compressive Strength History